



**HAL**  
open science

## Nonlinear Current Sheet Model of Electrical Machines

Jiling Guo, Loic Queval, Bastien Roucaries, Lionel Vido, Li Liu, Frédéric Trillaud, Christophe Berriaud

► **To cite this version:**

Jiling Guo, Loic Queval, Bastien Roucaries, Lionel Vido, Li Liu, et al.. Nonlinear Current Sheet Model of Electrical Machines. IEEE Transactions on Magnetics, 2020, 56 (1), pp.1-4. 10.1109/TMAG.2019.2950614 . hal-02464662

**HAL Id: hal-02464662**

**<https://hal.science/hal-02464662>**

Submitted on 3 Feb 2020

**HAL** is a multi-disciplinary open access archive for the deposit and dissemination of scientific research documents, whether they are published or not. The documents may come from teaching and research institutions in France or abroad, or from public or private research centers.

L'archive ouverte pluridisciplinaire **HAL**, est destinée au dépôt et à la diffusion de documents scientifiques de niveau recherche, publiés ou non, émanant des établissements d'enseignement et de recherche français ou étrangers, des laboratoires publics ou privés.

# Nonlinear Current Sheet Model of Electrical Machines

Jiling Guo<sup>1,2</sup>, Loïc Quéval<sup>2</sup>, Bastien Roucaries<sup>3</sup>, Lionel Vido<sup>3</sup>, Li Liu<sup>1</sup>, Frederic Trillaud<sup>4</sup>, Christophe Berriaud<sup>5</sup>

<sup>1</sup> School of Electrical Engineering, Southwest Jiaotong University, 610031 Chengdu, China

<sup>2</sup> GeePs, UMR CNRS 8507, CentraleSupélec, Univ. Paris-Sud, Univ. Paris-Saclay, Sorbonne Univ., 91192 Gif-sur-Yvette, France

<sup>3</sup> SATIE, CNRS UMR 8029, Univ. of Cergy Pontoise, 95000 Cergy-Pontoise, France

<sup>4</sup> Instituto de Ingeniería, Universidad Nacional Autónoma de México, 04510 CDMX, Mexico

<sup>5</sup> DRF/IRFU/DACM, CEA Saclay, Univ. Paris-Saclay, 91191 Gif-sur-Yvette, France

An incremental improvement of the classical semi-analytical current sheet model of electrical machines is proposed. First, it provides a better description of the current sheets that allows to consider, at the same time, the rotation of the rotor field winding and the time-dependent stator armature windings currents. This derivation is kept generic and the system to be solved is explicitly written in order to facilitate the implementation. Second, a refined iterative scheme that permits to account effectively for the nonlinearity of iron cores is introduced. It is demonstrated that the nonlinear current sheet model is particularly suitable for slotless wound rotor machines, being able to represent both the space harmonics and the saturation of the machine with a fair accuracy and computing speed compared to the nonlinear finite element model.

**Index Terms**—Electrical machine modeling and simulation, semi-analytical model, subdomain model, current sheet model, nonlinear material, slotless machine, air cored machine.

## I. INTRODUCTION

THE "CURRENT SHEET MODEL" is a semi-analytical model for the calculation of the magnetic field in an electrical machine. It belongs to the family of "subdomain models" ie. it is based on the formal resolution of Maxwell's equations in each subdomain [2]. Its distinctive feature is to divide the machine into annular subdomains and to model the windings as cylindrical current sheets. The Laplace's equation for the magnetic vector potential  $\mathbf{A}$  can then be solved analytically in each subdomain by the classic method of the separation of variables using appropriate boundary and interface conditions. Hugues and Miller pioneered this method in 1977 [3], [4]. At the time, they obtained concise analytical formulas for the field in the rotor core, air gap, stator core and air surrounding the machine. The method was later extended to add the shaft [5], [6], [7], the current sheets space harmonics [8] and the winding thickness [9]. Finally an iterative technique was introduced by Yazdani *et al.* [5], [6] to account for the nonlinearity of the iron. Despite those improvements, the latest models could not include directly several windings at the same time nor account for the rotation of the rotor.

The following work tackles this problem by expressing the current sheets not only as a classic sum of sines but as a sum of both sines and cosines. As a result, the proposed model can naturally include both the rotation of the rotor field winding and the time-dependent stator armature windings currents. In addition, an iterative scheme improved from [5], [6] is used to take into account the nonlinearity of the iron.

Manuscript submitted Aug 2019. Corresponding authors: L. Quéval (email: loic.queval@centralesupelec.fr) and F. Trillaud (ftrillaudp@pumas.ii.unam.mx). This work was supported by the grants: EolSupra20 project ANR-10-LABX-0040-LaSIPS, Chinese Scholarship Council and Fundamental Research Funds for the Centrale Universities under grants 2682018CX18, DGAPA-UNAM PAPIIT-2019 (#IN107119) and Programa de Apoyos para la Superación del Personal Académico of the UNAM (PASPA-DGAPA 2019).

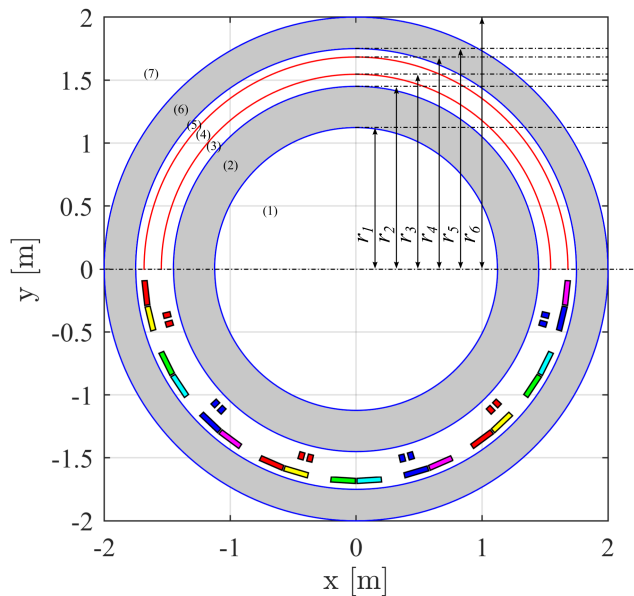


Fig. 1. (top) Machine generic geometry, (bottom) machine specific geometry.

## II. MODELING

### A. Machine geometry

The current sheet model assumes that the whole machine domain is divided into  $N$  concentric annular subdomains. For  $\ell \in [1, N]$ , the  $\ell^{\text{th}}$  subdomain has an inner radius  $r_{\ell-1}$ , an outer radius  $r_{\ell}$  and a relative permeability  $\mu_{r,\ell}$ . The boundary between the  $\ell^{\text{th}}$  domain and the  $(\ell+1)^{\text{th}}$  domain is a current sheet  $K_{\ell}(\theta)$  located at  $r = r_{\ell}$ .

To illustrate how the approach is applied to a specific machine, we considered the slotless wound rotor synchronous

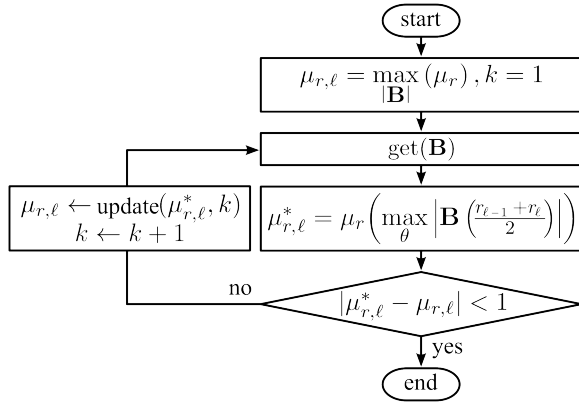


Fig. 2. Iterative scheme to determine the effective subdomain relative permeabilities  $\mu_\ell$  in the nonlinear case. The update operator designates the numerical damping.

machine with concentrated windings shown in Fig. 1. The current sheet model is particularly well suited for this kind of machine, but it has also been used for slotted machines [8].

### B. Equivalent current sheet $K_\ell(\theta)$

For a machine with  $P$  pairs of pole,  $K_\ell(\theta)$  is  $\frac{2\pi}{P}$ -periodic with a mean value equal to zero. Thus, it can be written as a Fourier series,

$$K_\ell(\theta) = \sum_{h=1}^{+\infty} [K_{\ell,h}^s \sin(hP\theta) + K_{\ell,h}^c \cos(hP\theta)] \quad (1)$$

where  $K_{\ell,h}^s$  and  $K_{\ell,h}^c$  are Fourier coefficients to be determined from the machine specific geometry.

### C. Field in the $\ell^{\text{th}}$ subdomain

In 2-D polar coordinates (neglecting the end effects), the magnetic vector potential  $\mathbf{A}$  has only one component along the  $z$ -axis and depends only on  $r$  and  $\theta$  coordinates. The resulting scalar potential  $A_z(r, \theta)$  is solution of Laplace's equation. Using the method of the separation of variables in the  $\ell^{\text{th}}$  annular subdomain and considering the current sheets to be expressed as (1), the scalar potential  $A_{z,\ell}(r, \theta)$  reduces to,

$$A_{z,\ell}(r, \theta) = \sum_{h=1}^{+\infty} \left[ (a_{\ell,h} r^{hP} + b_{\ell,h} r^{-hP}) \sin(hP\theta) + (c_{\ell,h} r^{hP} + d_{\ell,h} r^{-hP}) \cos(hP\theta) \right] \quad (2)$$

where  $a_{\ell,h}$ ,  $b_{\ell,h}$ ,  $c_{\ell,h}$  and  $d_{\ell,h}$  are coefficients to be determined. Knowing  $\mathbf{A}$  in each subdomain  $\ell$  with permeability  $\mu_\ell$ , we can derive the magnetic flux density  $\mathbf{B} = \nabla \times \mathbf{A}$  and the magnetic field strength  $\mathbf{H} = \mu_\ell^{-1} \mathbf{B}$ .

### D. Boundary and interface conditions

At  $r = 0$  ( $\ell = 1$ ), the boundary condition is,

$$A_{z,1}(0, \theta) = 0, \quad \forall \theta \quad (3)$$

At  $r = r_\ell$  ( $1 \leq \ell < N$ ), the interface condition is,

$$\begin{cases} B_{r,\ell+1}(r_\ell, \theta) - B_{r,\ell}(r_\ell, \theta) = 0 \\ H_{\theta,\ell+1}(r_\ell, \theta) - H_{\theta,\ell}(r_\ell, \theta) = K_\ell(\theta), \end{cases} \quad \forall \theta \quad (4)$$

At  $r = +\infty$  ( $\ell = N$ ), the boundary condition is,

$$A_{z,N}(+\infty, \theta) = 0, \quad \forall \theta \quad (5)$$

The boundary and interface conditions (3)-(5) constitute a system of  $4N$  equations that must be respected for each harmonic  $h$ . This system can be written as (6) of the form  $\mathbf{R}\mathbf{x} = \mathbf{b}$ . Being generic and explicit, the implementation of the current sheet model is straightforward [10].

### E. Resolution for linear and nonlinear cases

In the linear case, by inverting (6) numerically for each harmonic, one can obtain the potential  $A_{z,\ell}$  from (2). In the nonlinear case, the permeability  $\mu_\ell$  is a function of the magnetic flux density. In the current sheet model, the permeability  $\mu_\ell$  is modeled as uniform over the whole  $\ell^{\text{th}}$  subdomain. If this is not a limitation in the linear case, it becomes problematic when considering a nonlinear  $BH$  curve for the iron. Indeed, to preserve the accuracy of the model one should select an effective permeability that can represent well the non-uniformly magnetized core. Here, the fixed-point iteration procedure with numerical damping depicted in Fig. 2 has been implemented. Inspired by [5], [6], [11], this improved scheme computes the effective rotor permeability as the minimum of the permeability along the mean radius of the domain. Note that at each iteration, the  $\mu_\ell$  of the subdomain  $\ell$  is fixed. This allows us to solve a linear problem, where the different harmonics can be simply added.

## III. RESULTS

Because of its underlying modeling hypotheses, the current sheet model is naturally adapted to slotless wound rotor electrical machine. As an example, we investigate here the performance of the 12-pole 3-phase synchronous machine with concentrated windings shown in Fig. 1. Such a structure has been recently proposed for multi-MW fully superconducting wind turbine generators [12], [13]. The suppression of magnetic teeth is often considered for superconducting machines to cope with their large magnetic field (up to several Tesla), with the difficulty of winding superconducting materials and to simplify the cooling system. The machine parameters are summarized in Appendix together with the iron  $BH$  curve. For the current sheet model, 13 harmonic terms are included. For validation purpose, the results are compared to a nonlinear 2-D finite element (FE) model carried out in COMSOL Multiphysics.

### A. Equivalent current sheets

For the specific field winding arrangement of Fig. 1,  $K_3(\theta)$  is given by (1) with,

$$\begin{aligned} K_{3,h}^s &= \frac{8N_f i_f}{\pi w_f h} \sin\left(\frac{\theta_{1f} + \theta_{2f}}{2} h\right) \sin\left(\frac{\theta_{1f}}{2} h\right) \cos(hP\alpha) \\ K_{3,h}^c &= -\frac{8N_f i_f}{\pi w_f h} \sin\left(\frac{\theta_{1f} + \theta_{2f}}{2} h\right) \sin\left(\frac{\theta_{1f}}{2} h\right) \sin(hP\alpha) \end{aligned} \quad (7)$$

where  $h$  is odd,  $\alpha$  is the rotor mechanical angle,  $N_f$  is the number of turns of the rotor winding,  $i_f$  is the instantaneous

$$\begin{bmatrix}
0 & 1 & 0 & 0 & 0 & 0 & 0 & 0 \\
0 & 0 & 0 & 1 & 0 & 0 & 0 & 0 \\
& & R_{3,1} & & & & & \\
& & & \ddots & & & & \\
& & & & R_{4(\ell-1)+3,4(\ell-1)+1} & & & \\
& & & & & \ddots & & \\
& & & & & & R_{4(N-2)+3,4(N-2)+1} & \\
0 & 0 & 0 & 0 & 1 & 0 & 0 & 0 \\
0 & 0 & 0 & 0 & 0 & 0 & 1 & 0
\end{bmatrix}
\times
\underbrace{\begin{bmatrix} x_1 \\ x_2 \\ \vdots \\ x_{4(\ell-1)+1} \\ \vdots \\ x_{N-1} \\ x_N \end{bmatrix}}_{\mathbf{x}_{4N \times 1}} =
\underbrace{\begin{bmatrix} 0 \\ 0 \\ K_3 \\ \vdots \\ K_{4(\ell-1)+3} \\ \vdots \\ K_{4(N-2)+3} \\ 0 \\ 0 \end{bmatrix}}_{\mathbf{b}_{4N \times 1}}$$

$$R_{4(\ell-1)+3,4(\ell-1)+1} = \begin{bmatrix}
-r_\ell^{hP} & -r_\ell^{-hP} & 0 & 0 & r_\ell^{hP} & r_\ell^{-hP} & 0 & 0 \\
0 & 0 & -r_\ell^{hP} & -r_\ell^{-hP} & 0 & 0 & r_\ell^{hP} & r_\ell^{-hP} \\
r_\ell^{hP} & r_\ell^{-hP} & 0 & 0 & -r_\ell^{hP} & -r_\ell^{-hP} & 0 & 0 \\
\mu_\ell & \mu_\ell & 0 & 0 & \mu_{\ell+1} & \mu_{\ell+1} & 0 & 0 \\
0 & 0 & r_\ell^{hP} & -r_\ell^{-hP} & 0 & 0 & -r_\ell^{hP} & r_\ell^{-hP} \\
& & \mu_\ell & \mu_\ell & & & \mu_{\ell+1} & \mu_{\ell+1}
\end{bmatrix}_{4 \times 8}$$

$$x_{4(\ell-1)+1} = \begin{bmatrix} a_{\ell,h} \\ b_{\ell,h} \\ c_{\ell,h} \\ d_{\ell,h} \end{bmatrix}_{4 \times 1} \quad K_{4(\ell-1)+3} = \frac{1}{hP} \begin{bmatrix} 0 \\ 0 \\ K_{\ell,h}^s r_\ell \\ K_{\ell,h}^c r_\ell \end{bmatrix}_{4 \times 1} \quad (6)$$

where  $1 \leq \ell < N$ .

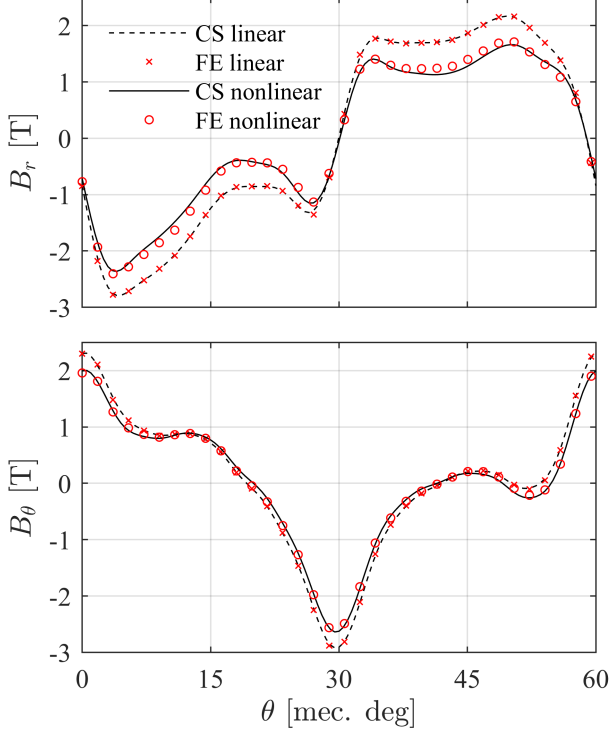


Fig. 3. Comparison of the air-gap (top) radial and (bottom) azimuthal components of the magnetic flux density for the current sheet (CS) model and the finite element (FE) model ( $r = r_{Te}$ ).

field coil current,  $\theta_{1f}$  is the coil width electrical angle,  $\theta_{2f}$  is the coil aperture electrical angle and  $w_f$  is the coil width.

Similarly, for the specific armature winding arrangement of Fig. 1,  $K_4(\theta)$  is given by (1) with,

$$\begin{aligned}
K_{4,h}^s &= \frac{4N_a}{\pi w_a h} \sin\left(\frac{\theta_{1a} + \theta_{2a}}{2} h\right) \sin\left(\frac{\theta_{1a}}{2} h\right) \\
&\quad \times \left[ i_a + i_b \cos\left(h \frac{2\pi}{3}\right) + i_c \cos\left(h \frac{4\pi}{3}\right) \right] \\
K_{4,h}^c &= -\frac{4N_a}{\pi w_a h} \sin\left(\frac{\theta_{1a} + \theta_{2a}}{2} h\right) \sin\left(\frac{\theta_{1a}}{2} h\right) \\
&\quad \times \left[ i_b \sin\left(h \frac{2\pi}{3}\right) + i_c \sin\left(h \frac{4\pi}{3}\right) \right]
\end{aligned} \quad (8)$$

where  $N_a$  is the number of turns of the armature windings,  $(i_a, i_b, i_c)$  are the instantaneous 3-phase currents,  $\theta_{1a}$  is the coil width electrical angle,  $\theta_{2a}$  is the coil aperture electrical angle and  $w_a$  is the coil width.

### B. Load condition

For the load condition, the following parameters are used:  $i_f = 5.03$  kA,  $i_a = -1.53$  kA,  $i_b = 2.465$  kA,  $i_c = -0.935$  kA,  $\alpha = -15^\circ$ . The magnetic flux density in the air gap is plotted in Fig. 3. Fig. 4 shows the magnetic flux density distribution in the whole domain. In the linear case, the agreement between the current sheet model and the FE model is very good. In the nonlinear case, the agreement is good for the field in the air gap and fair for the field distribution. The discrepancy is mainly attributed to the impossibility of modeling the azimuthal variation of  $\mu_\ell$  for the current sheet

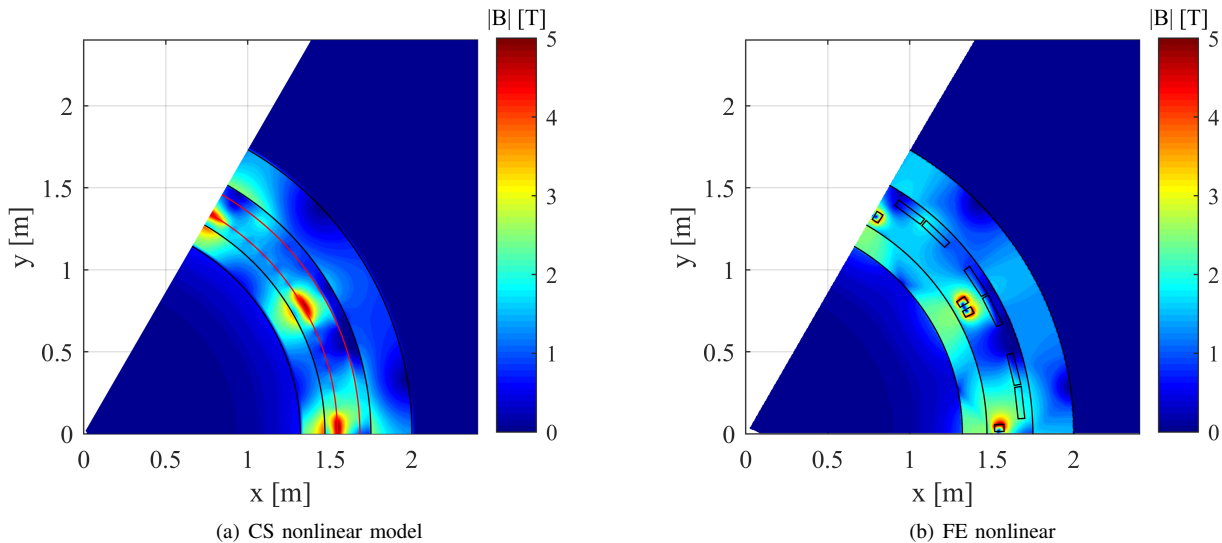


Fig. 4. Comparison of the magnetic flux density distribution for the current sheet (CS) model and the finite element (FE) model (load condition at  $t = 0$  s).

model. The computation time for the nonlinear current sheet model is about 1.3 s (roughly 100 ms per iteration, <15 iterations) on an i7-5600 CPU @2.60 Ghz, 16 GB RAM. This is about 5 times faster than the nonlinear FE model, using symmetries to reduce the mesh to 9220 elements. Note that an efficient implementation of the current sheet model could lead to an even lower computing time [14].

#### IV. CONCLUSION

In comparison to previous current sheet models, the present derivation sets itself apart by its genericity. It accounts simultaneously for the rotor rotation and the time-dependent stator currents. In addition, the nonlinearity of the cores is included thanks to an iterative procedure. It provides the end user with a simple model that can be quickly implemented in any freely-available programming languages to carry out pre-design and optimization studies of slotless wound rotor electrical machines. It is adapted to a wide range of designs, including multiphase machines with multi-layer distributed or concentrated windings.

#### APPENDIX MACHINE PARAMETERS

$r_1 = 1.320$  m,  $r_2 = 1.470$  m,  $r_3 = 1.546$  m,  $r_4 = 1.683$  m,  $r_5 = 1.750$  m,  $r_6 = 2.000$  m,  $\mu_1 = \mu_3 = \mu_4 = \mu_5 = \mu_7 = \mu_0$ ,  $\mu_2 = \mu_6 = \mu_0 \mu_r(|\mathbf{B}|)$ ,  $K_1 = K_2 = K_5 = K_6 = 0$ ,  $P = 6$ ,  $h_f = 0.057$  m,  $w_f = 0.042$  m,  $\theta_{1f} = 0.163$  elec. rad,  $\theta_{2f} = 2.703$  elec. rad,  $h_a = 0.041$  m,  $w_a = 0.194$  m,  $\theta_{1a} = 0.692$  elec. rad,  $\theta_{2a} = 0.664$  elec. rad,  $L_{eff} = 1.540$  m,  $N_a = 120$ ,  $N_f = 100$ ,  $r_{Te} = 1.619$  m.  $(B, H) = [(1.0, 663), (1.1, 1067), (1.2, 1705), (1.3, 2463), (1.4, 3841), (1.5, 5425), (1.6, 7957), (1.7, 12298), (1.8, 20462), (1.9, 32169), (2.0, 61213), (2.1, 111408), (2.3, 500000), (2.6, 1500000), (5, 3978900)]$ .  $B$  in T,  $H$  in  $A \cdot m^{-1}$ .

#### REFERENCES

- [1] B.L.J. Gysen, K.J. Meessen, J.J.H. Paulides, E.A. Lomonova, "General formulation of the electromagnetic field distribution in machines and devices using fourier analysis," *IEEE Trans. on Magnetics*, vol. 46, no. 1, pp. 39-52, 2010.
- [2] E. Devillers, J. Le Besnerais, T. Lubin, M. Hecquet, J.-P. Lecoq, "A review of subdomain modeling techniques in electrical machines: performances and applications," *22th Intl. Conf. Elec. Machines ICEM2016*, pp. 86-92, Lausanne, Switzerland, 2016.
- [3] A. Hughes, T.J.E. Miller, "Analysis of fields and inductances in air-cored and iron-cored synchronous machines," *Proc. Inst. Elect. Eng.*, vol. 124, no. 2, pp. 121-126, 1977.
- [4] T.J.E. Miller, A. Hughes, "Comparative design and performance analysis of air-cored and iron-cored synchronous machines," *Proc. Inst. Elect. Eng.*, vol. 124, no. 2, pp. 127-132, 1977.
- [5] P. Elhaminia, M. Yazdani, M.R. Zolghadri, M. Fardmanesh, "An analytical approach for optimal design of rotor iron for superconducting synchronous machine," *37th Annual Conf. IEEE Industrial Electronics Society IECON2011*, Melbourne, Australia, pp. 1741-1745, 2011.
- [6] M. Yazdani, P. Elhaminia, M.R. Zolghadri, M. Fardmanesh, "Analytical modeling of magnetic flux in superconducting synchronous machine," *IEEE Trans. on Applied Superconductivity*, vol. 23, no. 1, id. 5200406, 2013.
- [7] W. Zhang, D. Xia, D. Zhang, G. Zhang, "Parameter design by a novel method and optimization of the field coil for a 500 kW air-gap HTS generator," *IEEE Trans. on Applied Superconductivity*, vol. 24, no. 3, id. 5201704, 2014.
- [8] J.R. Bumby, *Superconducting Rotating Electrical Machines*. Oxford, U.K.: Clarendon, 1983.
- [9] S. Safi, J. Bumby, "Analysis of magnetic fields in the slotted structure of a superconducting AC generator," *Proc. Inst. Elect. Eng.*, vol. 139, no. 5, pp. 411-422, 1992.
- [10] CS model, 2019. [Online]. Available: <https://github.com/lqueval/CS>. [Accessed Oct. 28, 2019].
- [11] Z. Djelloul-Khedda, K. Boughrara, F. Dubas, R. Ibtouen, "Nonlinear analytical prediction of magnetic field and electromagnetic performances in switched reluctance machines," *IEEE Trans. on Magnetics*, vol. 53, no. 7, pp. 1-11, 2017.
- [12] Y. Terao, M. Sekino, H. Ohsaki, "Electromagnetic design of 10 MW class fully superconducting wind turbine generators," *IEEE Trans. on Applied Superconductivity*, vol. 22, no. 3, pp. 5201904, 2012.
- [13] T.-K. Hoang, L. Queval, C. Berriaud, L. Vido, "Design of a 20 MW fully superconducting wind turbine generator to minimize the levelized cost of energy," *IEEE Trans. on Applied Superconductivity*, vol. 28, no. 4, pp. 1-4, 2018.
- [14] A. Gilson, S. Tavernier, F. Dubas, D. Depernet, C. Espanet, M.M. Technologies, "2-D analytical subdomain model for high speed permanent-magnet machines," *18th Intl. Conf. Elec. Machines and Systems ICEMS2015*, pp. 1508-1514, Pattaya, Thailand, 2015.